J Solid State Electrochem (2012) 16:795–802
DOI 10.1007/s10008-011-1431-7

ORIGINAL PAPER

Fabrication of gold nanoparticles/polypyrrole composite-modified electrode for sensitive hydroxylamine sensor design

Jing Li · Huaqing Xie · Yang Li

Received: 20 December 2010 / Revised: 2 May 2011 / Accepted: 5 May 2011 / Published online: 20 May 2011

Abstract A highly sensitive hydroxylamine (HA) electrochemical sensor is developed based on electrodeposition of gold nanoparticles with diameter of 8 nm on the pre-synthesized polypyrrole matrix and formed gold nanoparticles/polypyrrole (GNPs/PPy) composite on glassy carbon electrode. The electrochemical behavior and electrocatalytic activity of the composite-modified electrode are investigated. The GNPs/PPy composite exhibits a distinctly higher electrocatalytic activity for the oxidation of HA than GNPs with twofold enhancement of peak current. The enhanced electrocatalytic activity is attributed to the synergic effect of the highly dispersed gold metal particles and PPy matrix. The overall numbers of electrons involved in HA oxidation, the electron transfer coefficient, catalytic rate constant, and diffusion coefficient are investigated by chronoamperometry. The sensor presents two wide linear ranges of 4.5×10^{-7}–1.2×10^{-3} M and 1.2×10^{-3}–19×10^{-3} M with the detection limit of 4.5×10^{-8} M (s/n=3). In addition, the proposed electrode shows excellent sensitivity, selectivity, reproducibility, and stability properties.

Keywords Electrocatalytic oxidation · Polypyrrole · Gold nanoparticles · Hydroxylamine · Electrodeposition

Introduction

In the past decades, nanostructured materials have been investigated extensively because of their fascinating chemical, optical, and electronic properties [1, 2]. Nanoparticles have extraordinarily catalytic activities toward both oxidation and reduction reactions. Particularly, gold nanoparticles (GNPs) have been used increasingly in many electrochemical applications because the nano-sized GNPs have the ability to enhance the electrode conductivity, facilitate the electron transfer rate, and improve the analytical sensitivity [1, 3–6]. However, the electrocatalytic properties of GNPs mostly depend on the size, shape, and supporting materials [7].

Composite of conducting polymers and inorganic nanoparticles has attracted growing attention due to its unique properties in several applications [8–10]. Many researches have been devoted to investigating the dispersion of inorganic particles in thin films of various polymers [5, 8]. In particular, polypyrrole (PPy) is one of the most extensively used conducting polymers because of its high electronic conductivity, easy preparation, good environmental stability, and large variety of applications [11–14]. Up to now, various morphologies of PPy have been synthesized and assembled, such as nanofibers [15], nanowires [16], nanotubes [17], and nanoparticles [18]. PPy are usually employed as matrix to embed noble metal particles for the electro-oxidation of small molecules [19–22]. As a porous structure matrix, PPy could not only provide low ohmic drops but also enhance the rate constant of electron transfer process for several electroactive species.

Hydroxylamine (HA) is known as a kind of reducing reagent, which is commonly used in industrial processes. It is also used as a raw material for synthesis of pharmaceutical intermediates and final drug substances [23]. HA has been identified as one of the intermediate products in many biological processes and production of nitrous oxide [24]. However, it is a well-known mutagen, moderately toxic, and harmful to humans, animals, and plants [25]. Therefore,

J. Li · H. Xie (✉) · Y. Li
School of Urban Development and Environmental Engineering,
Shanghai Second Polytechnic University,
Shanghai 201209, People's Republic of China
e-mail: hqxie@eed.sspu.cn

it is necessary to develop a sensitive analytical method for detecting low levels of HA [26].

Recently, numerous methods have been used to determine HA, such as ion chromatography [23], spectrophotometry [27, 28], capillary electrophoresis [29], gas chromatography [30], and biamperometry [31]. However, the processes involved in many of these methods are extremely complex and the linear ranges are relatively narrow. Electroanalytical techniques offer the opportunity for simple, direct, and effective detection of HA [32]. Unfortunately, HA exhibits irreversible oxidation requiring large overpotential at most conventional electrodes. One of the promising approaches is the use of chemically modified electrodes (CMEs). Various CMEs has been constructed and applied in HA determination [5, 33–35].

In the present work, a new HA sensor was fabricated based on the electrodeposition of GNPs onto pre-synthesized PPy nanoparticles. The GNPs with diameter of 8 nm dispersed uniformly on the PPy particles matrix. The GNPs/PPy composite showed an excellent electrocatalytic activity toward the oxidation of HA by improving its oxidation current for about two times with 80 mV less-positive potential shift while compared to GNPs-modified glassy carbon electrode (GNPs/GCE).

Experimental

Materials

HA, $FeCl_3$, and $HAuCl_4$ were obtained from Chemical Reagent Company of Shanghai (Shanghai, China). Pyrrole was obtained from Aldrich and purified twice by distillation under the protection of high-purity nitrogen and then kept in a refrigerator before use. Dodecylsulfate sodium was obtained from Sino-American Biotechnology Company. All other chemicals were analytical grade and were used without further purification. The 0.1 M phosphate buffer solutions of different pH values (PBSs) were prepared as the electrolytes. All electrochemical experiments were carried out at ambient temperature. Doubly distilled water was used to prepare solutions.

Apparatus

All electrochemical measurements were conducted on CHI 660C electrochemical workstation (ChenHua Instruments Co., Shanghai, China). A conventional three-electrode electrochemical system was used. A glassy carbon-modified electrode (GCE, Φ4.0 mm) was used as working electrode, a platinum wire as counter electrode and a saturated calomel electrode as reference electrode. Electrochemical impedance spectroscopy (EIS) was obtained in 10 mM $K_3[Fe(CN)_6]/K_4[Fe(CN)_6]$ (1:1 mixture) solution containing 0.1 mol/L KCl in a electrochemical cell with a netted Pt counter electrode of about 2-cm^2 surface area.

The images of the electrode surfaces were carried out with JSM-6700F field emission scanning electron microanalyser (FE-SEM; JEOL, Japan). Powder X-ray diffraction (XRD) spectra was recorded on a MXPAHF rotating anode X-ray diffractometer (Japan) with Cu-Kα radiation source ($\lambda = 1.54056$ Å).

Synthesis of PPy nanoparticles

PPy nanoparticles were synthesized as following methods: under stirring, 7.5 mmol of dodecylsulfate sodium was dissolved in 150 ml of doubly distilled water. The water was purged with highly pure nitrogen for 30 min before experiment, in order to obtain completely saturated nitrogen solution. Pyrrole monomer (0.33 mL) was added to above solution and the reaction was allowed to proceed for 2 h at 0 °C (in an ice bath) under stirring. After that, 0.02 mol of ferric chloride was added into the solution. The polymerization reaction was subjected to high-speed stirring for 5 h. The resulting product was washed with water and methanol repeatedly and then centrifuged at 5,000 rpm for 10 min. Then, the product was dried in a vacuum oven at 30 °C for 24 h. Finally, PPy powder was obtained.

Electrode preparation

Prior to modification, the basal GCE was carefully polished with 1.0, 0.3, and 0.05-μm alumina powder slurries, and then treated in ethanol and doubly distilled water in an ultrasonic bath for 5 min, respectively, in order to remove any adsorbed substances at the electrode surface. Then, it was dried under nitrogen atmosphere ready for use.

Synthesized PPy (10 mg) was added into 10 mL of ethanol under ultrasonic agitation to obtain a black suspension. PPy suspension (10 μL) was dripped onto the fresh GCE surface and naturally dried in room temperature to form PPy-modified GCE (PPy/GCE). The PPy/GCE was used as the working electrode to deposited GNPs. The electrochemical deposition was performed in 0.1 M KCl solution containing 0.5 mM $HAuCl_4$ by cycling potential between 0.2 and −0.8 V for 15 cycles at 50 mV s^{-1}. The amount and the size of the GNPs can be controlled through changing the cycle number in electrodeposition process. Considering the particle size would influence the catalytic efficiency, the optimum cycle number was chosen as 15 cycles. The generated GNPs/PPy composite film-modified GCE was obtained and denoted as GNPs/PPy/GCE. For comparison, GNPs/GCE was also prepared under the same conditions.

Results and discussion

Characterization of the GNPs/PPy composite film

The morphology of developed PPy is characterized by FE-SEM. As seen in Fig. 1a, the synthesized PPy shows evident nanoparticles image. The average diameter is about 40 nm. These particles are linked and packed together. Furthermore, the image reveals that the surfaces of PPy samples possess rough and extended porous structures. Figure 1b illustrates the image of the GNPs/PPy composite. The spherical GNPs of 8 nm are well dispersed on the PPy nanoparticles surface without significant aggregation.

The presence of Au in the nanocomposite was further confirmed by powder XRD measurement, as shown in Fig. 2. In the XRD curve of the GNPs/PPy composite (curve a), a broad peak observed at 23.8° related to the amorphous PPy, which is similar to the conventional PPy (as seen in curve b). Moreover, four bands appeared with maximum intensity at 38.1°, 44.4°, 64.5°, and 77.5°, which are assigned to the diffractions of the (111), (200), (220), and (311) planes of Au, demonstrating the face-centered cubic metal gold structure is formed. In addition, the composite was also investigated by XPS determination. The Au 4f spectrum consisting of two peaks observed at 83.9 and 87.6 eV, corresponding to the Au $4f_{7/2}$ and Au $4f_{5/2}$ components.

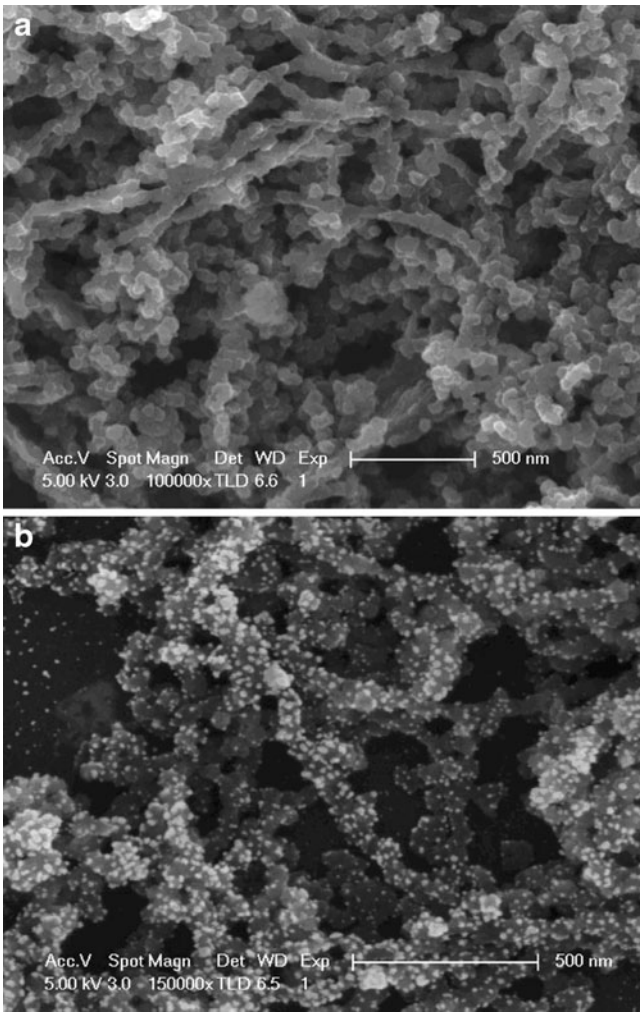

Fig. 1 FE-SEM images of PPy nanoparticles (**a**) and GNPs/PPy composite (**b**) on bare GCE

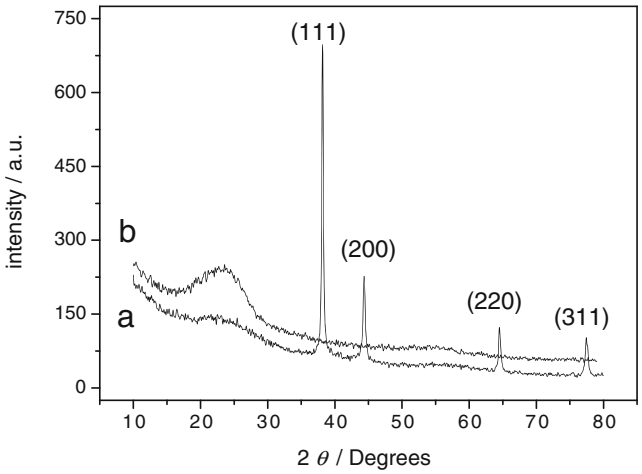

Fig. 2 XRD pattern of GNPs/PPy composite (*curve a*) and PPy nanoparticles (*curve b*)

EIS is a powerful and informative technique to examine the properties of surface-modified electrode. In the Nyquist plots, the semicircular portion of the impedance spectrum at higher frequency represents the charge transfer-limited process, and the diameter of the semicircle equals to the surface charge transfer resistance (R_{ct}). The R_{ct} value depends on the dielectric and insulting properties of the electrode/electrolyte solution interface [36]. The EIS at the bare GCE, PPy/GCE, GNPs/GCE, and GNPs/PPy/GCE were illustrated in Fig. 3. Significant difference of R_{ct} value is observed at the modified electrodes. The R_{ct} value of the bare GCE (curve a) is 1,500 Ω. The diameter of the high frequency semicircle is apparently reduced at the PPy/GCE and the R_{ct} value is 780 Ω (curve b). The significant decrease of R_{ct} value might be due to the presence of PPy nanoparticles, which played an important role in accelerating the transfer of the electrons. After dispersing GNPs on the bare GCE, the R_{ct} value decreased to 280 Ω (curve c), implying that GNPs was more facile to enhance the electron transfer due to its good electron conductivity. For the GNPs/PPy/GCE, the R_{ct} value (about 190 Ω) decreased further (curve d). These facts suggest that the charge transfer is faster at the GNPs/PPy/GCE in comparison with that at the GNPs/GCE and PPy/GCE, which facilitates the electron transfer between the electrochemical probe and the electrode surface. The results illustrate that PPy nanoparticles not only serve as a supporting material for GNPs

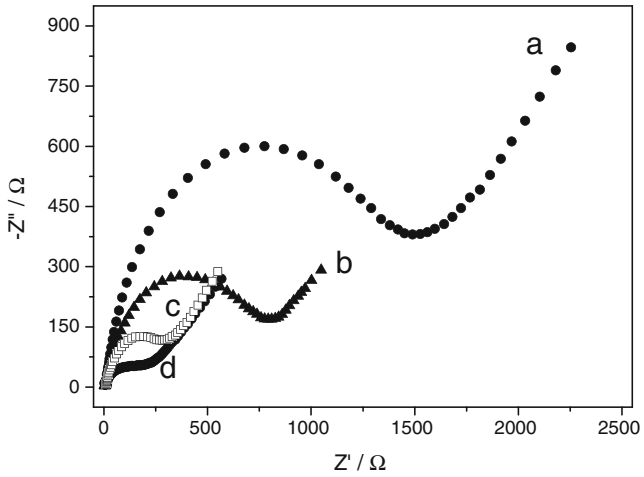

Fig. 3 EIS at the bare GCE (*a*), PPy/GCE (*b*), GNPs/GCE (*c*), and GNPs/PPy/GCE (*d*) in 10.0 mM $K_3[Fe(CN)_6]/K_4[Fe(CN)_6]$ (1:1 mixture)+0.1 M KCl

deposition but also can increase the electron transfer rate. The impedance change of the modification process indicates that PPy and GNPs have been successfully immobilized at the GCE surface.

Electrochemical oxidation of HA

The electrochemical behavior of HA was in detail investigated by cyclic voltammetry (CV) in 0.1 M PBS (pH 7.0). CVs are obtained in comparison with bare GCE, PPy/GCE, GNPs/GCE, and GNPs/PPy/GCE in the presence of 2.0×10^{-4} M HA. As seen in Fig. 4, at the bare GCE, there is no anodic peak current for HA oxidation (curve a). Under the same experimental conditions, PPy/GCE only makes the oxidation current slightly larger than that at the bare electrode, but no defined anodic peak is observed (curve b), which is attributed to the slow electron transfer kinetics of HA oxidation process. There is a dramatic enhancement of the oxidation current at the GNPs/GCE relative to the value obtained at the PPy/GCE and the bare GCE (curve c). The electro-oxidation of HA at the GNPs/GCE shows an irreversible wave. The oxidation peak potential appears at 0.29 V. The large decrease in oxidation overpotential corresponds to the presence of high density arrays of GNPs and its electrocatalytic behavior, which can improve reversibility of the electron transfer process. Furthermore, the GNPs/PPy/GCE shows a novel electrocatalytic oxidation towards HA (curve d). A well-formed sharp catalytic oxidation peak is observed at the potential of 0.21 V. The current response is much higher than that of the GNPs/GCE, indicating that the combination of PPy nanoparticles and GNPs definitely promote the electron transfer during HA electro-oxidation process. The above results demonstrate that PPy can be used as new supporting matrix for dispersing GNPs, in which GNPs have contributed significantly to the electrocatalytic process.

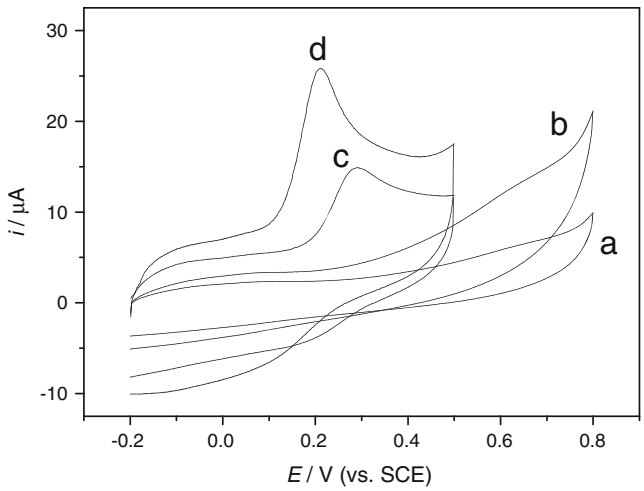

Fig. 4 CVs of 2.0×10^{-4} M HA in 0.1 M PBS at bare GCE (*curve a*), PPy/GCE (*curve b*), GNPs/GCE (*curve c*), and GNPs/PPy/GCE (*curve d*). Scan rate: 50 mV s^{-1}

The scan rate effect on the CV response of 2.0×10^{-4} M HA at GNPs/PPy/GCE was investigated. The anodic peak current increased with increasing the scan rate. A good linear relationship between anodic peak current and the square root of scan rate ($v^{1/2}$) is obtained in the range of 10 to 400 mV s^{-1}, indicating HA oxidation at GNPs/PPy/GCE is a typical diffusion-controlled process. In addition, the plot of scan rate normalized current ($i_p v^{-1/2}$) versus scan rate is observed, which exhibits characteristic typical shape of electrocatalysis catalytic process.

The oxidation peak potential (E_p) shifted toward positive direction with increasing the scan rate. A Tafel slope ($b=2.3RT/(1-\alpha)n_\alpha F$) of 114 mV $decade^{-1}$ was observed according to the linear relationship between E_p and log (v), consistent with one electron transfer process in the rate-determining step ($n_\alpha=1$). The charge transfer coefficient (α) was calculated as 0.49. From the slope of the I_p versus $v^{1/2}$ plot, the number of electrons (n) involved in the overall reaction can be obtained. According to the following equation for a totally irreversible diffusion-controlled process [37]:

$$I_p = 3.01\times10^5 n[(1-\alpha)n_\alpha]^{1/2} A c_b D^{1/2} v^{1/2}$$

where A is electrode surface area, c_b is HA concentration and D is diffusion coefficient. Considering $D=2.95\times10^{-5}$ cm^2 s^{-1} (D is calculated from chronoamperometry), the n involved in the oxidation is evaluated to be 2. Two electrons are involved in the oxidation process of HA at GNPs/PPy/GCE, which leads to the product of N_2O as shown in following reaction:

$$NH_2OH \rightarrow 1/2N_2O + 1/2H_2O + 2H^+ + 2e^-$$

Chronoamperometric measurements

In order to elucidate the kinetic of HA oxidation at GNPs/PPy/GCE, chronoamperometry is employed for the investigation of electrode process. Chronoamperometric measurements of different concentrations of HA are carried out for determination of diffusion coefficient (D) by setting the working electrode potential at 0.25 V. The diffusion coefficient can be evaluated according to the Cottrell equation [37]:

$$i = nFAD^{1/2}c/\pi^{1/2}t^{1/2}$$

where D and c are the diffusion coefficient (centimeter squared per second) and bulk concentrations (moles per cubic centimeter) of the analyte, respectively.

Chronoamperometry was recorded in 0.1 M PBS containing different concentrations of HA in the range of 5–200 μM. Figure 5a presents the experimental plots of i versus $t^{-1/2}$ with the best fits for various HA concentrations. The slopes of the resulting straight line are then plotted versus HA concentrations (inset in Fig. 5a). From the slope of the plot and using the Cottrell equation, the D is calculated to be 2.95×10^{-5} cm^2 s^{-1}. The value is higher than that reported previously for oxidation of HA [38].

The overall electrochemical oxidation of HA at GNPs/PPy/GCE is controlled by diffusion of the analytes in bulk solution and the cross-exchange process between the molecules and the redox sites of the composite film. The catalytic current is dominated by the rate of electrocatalyzed oxidation of HA. The value of the catalytic rate constant (k) can be evaluated using chronoamperometry based on the equation of $I_c/I_d=(\pi\ kc\ t)^{1/2}$, where I_d is the diffusion limited current in the absence of HA, I_c is the catalytic current in the presence of HA and c is the bulk concentration. On the slope of the I_c/I_d versus $t^{1/2}$ plot, as shown in Fig. 5b, the value of k is calculated as 2.91×10^4 $M^{-1}s^{-1}$, which is higher than the literature reported [33].

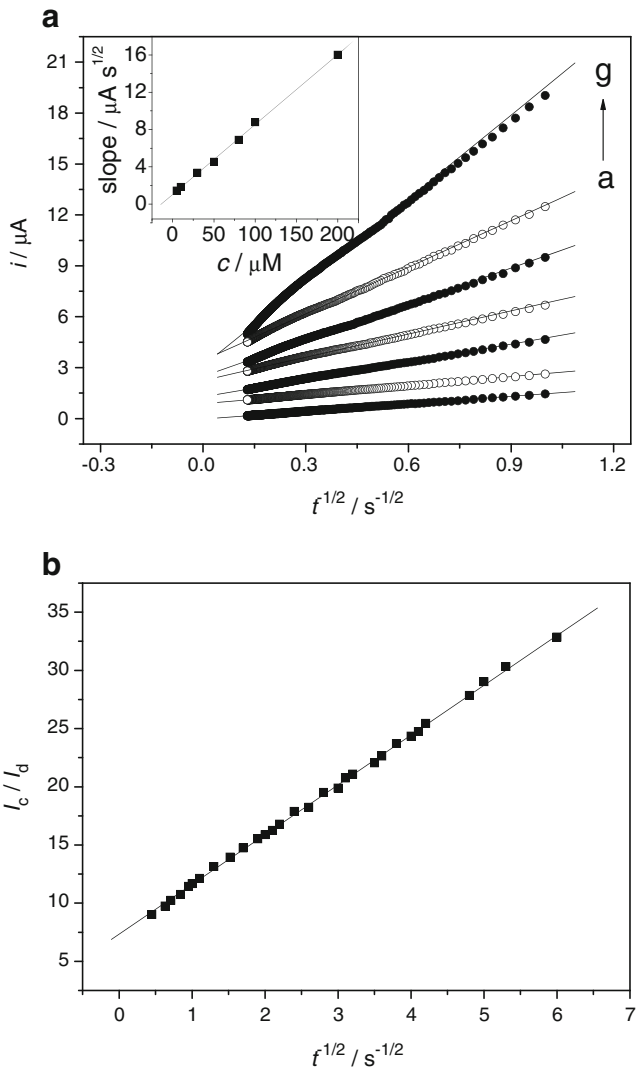

Fig. 5 (**a**) Plot of i versus $t^{-1/2}$ obtained from chronoamperometric measurements at the GNPs/PPy/GCE with different concentrations of HA ($a\rightarrow g$): 5.0×10^{-6}–2.0×10^{-4} M. *Inset* shows the relationship between the slopes of the linear segments and corresponding concentrations of HA. (**b**) Plots of I_c/I_d versus $t^{1/2}$, obtained from the data of chronoamperometric response on the GNPs/PPy/GCE in the presence and absence of 2.0×10^{-4} M HA

Effect of solution pH on the oxidation of HA

Generally, the electrochemical reaction is dependent on the pH value of aqueous solutions. Thus, the influence of pH on the electrochemical behavior of HA was investigated, as shown in Fig. 6. It can be seen that the catalytic peak current (i_{pa}) increases remarkably with increasing pH from 4 to 7.5 and then increases indistinctively. Since the pK_a of HA is 5.9, it presents two forms in solution, the non-protonated form NH_2OH for pH value higher than 5.9 and protonated form NH_3OH^+ at lower pH than 5.9. The decrease in peak current at lower pH was attributed to the protonation of HA, because the protonated form is less active. Considering the practically applications, pH 7.0 PBS was chosen as the supporting electrolyte in the electrochemical detection of HA.

Determination of HA

Differential pulse voltammetry (DPV) technique was used for determination of HA in static solutions. Very well-defined voltammograms are obtained at GNPs/PPy/GCE, as seen in Fig. 7a. The oxidation current increases while increasing the concentrations of HA. The plot of current responses (i_{pa}) versus concentration of HA is shown in Fig. 7b. A good linearity consisted of two segments is

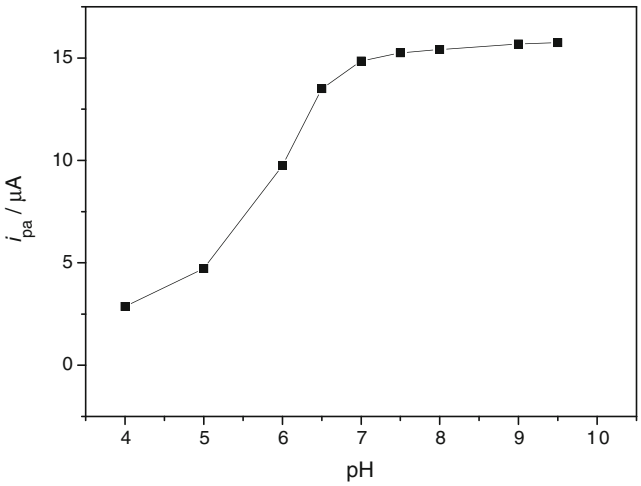

Fig. 6 Dependence of DPV anodic peak current at the GNPs/PPy/GCE on the solution pH in 0.1 M PBS in the presence of 2.0×10^{-4} M HA. Scan rate: 50 mV s^{-1}

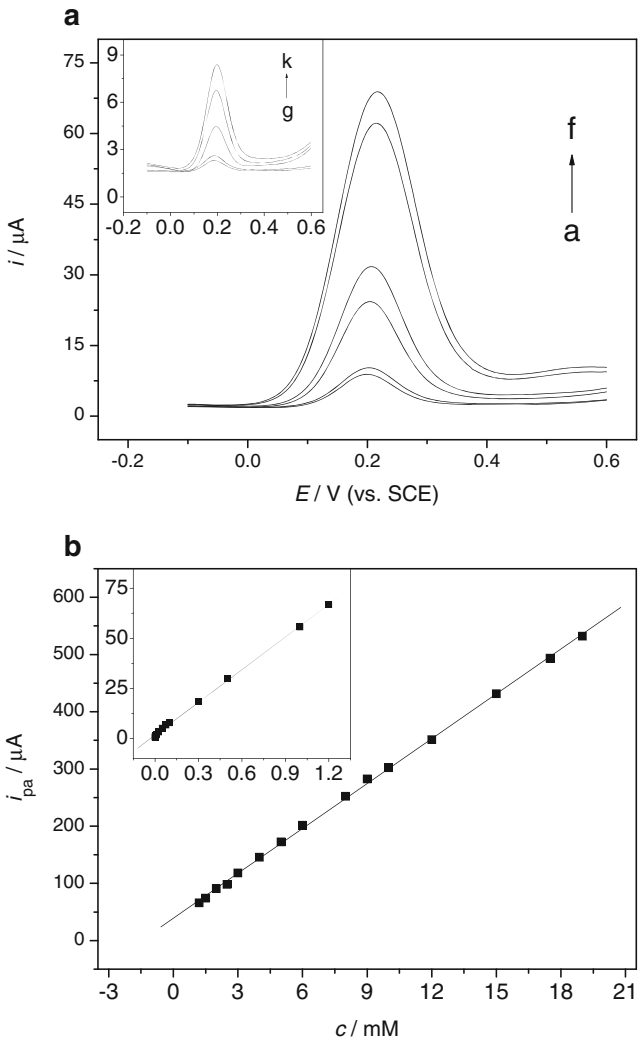

Fig. 7 (**a**) DPVs of different concentrations of HA at GNPs/PPy/GCE (a→f): 7.5×10^{-5}, 1.0×10^{-4}, 3.0×10^{-4}, 5.0×10^{-4}, 1.0×10^{-3}, 1.2×10^{-3} M. *Inset* presents DPVs of low concentrations (g→k): 4.5×10^{-7}, 1.0×10^{-6}, 1.0×10^{-5}, 2.5×10^{-5}, 5.0×10^{-5} M. (**b**) The corresponding calibration curves for HA (1.2×10^{-3}–19×10^{-3} M). *Inset* is the low concentrations of HA (4.5×10^{-7}–1.2×10^{-3} M)

obtained in wide concentrations range of 4.5×10^{-7}–1.2×10^{-3} M with a current sensitivity of 54.45 μA mM^{-1} and in the range of 1.2×10^{-3}–19×10^{-3} M with current sensitivity of 26.15 μA mM^{-1}. According to the former calibration plot, the detection limit is evaluated as 4.5×10^{-8} M (s/n= 3). The observed wide linear range with high sensitivity at GNPs/PPy/GCE indicates that the electrode can be successfully used for the determination of HA.

The analytical characteristics of the designed electrode are compared with those electrodes reported in the literature, as listed in Table 1. It can be seen that the designed GNPs/PPy/GCE has relatively low detection limit, high current sensitivity, and two linear regions covered wide determination ranges, demonstrating the proposed electrode is superior. Through a suitable combination of PPy nanoparticles matrix and well-dispersed GNPs, the GNPs/PPy composite can provide a porous nanostructure with large effective surface area and highly electrocatalytic activities toward the oxidation of HA. The PPy matrix not only can efficiently transfer electrons between the electrode and GNPs active sites, but also can reduce the adsorbed intermediates at the GNPs catalytic sites, preventing the modified electrode from fouling. Additionally, the supporting PPy matrix could reduce the congregating tendency of GNPs into large particles and finely disperse the GNPs.

Effect of interferents

The important problem to determine HA is the interference of other electroactive nitrogen containing compounds, such as nitrate, nitrite, ammonia, and hydrazine, which often accompany with HA in various industrial processes. The determination of HA in the presence of these common interferents has been investigated. The tolerance limit of the potentially interfering substances is defined as the molar ratio of the additive/HA causing relative error less than 5% for the determination of 1.0×10^{-5} M HA. The results show that 400-fold quantities of NO_3^-, NO_2^-, tenfold quantities of NH_3^+, and onefold quantities of hydrazine have no interference on the determination of HA. Furthermore, we have also checked the interfering effect of other common ions. No interference was observed with common cations and anions, for instance, 300-fold quantities of Cl^-, Br^-, F^-, I^-, HCO_3^-, PO_4^{3-}, CO_3^{2-}, $C_2O_4^{2-}$, SO_4^{2-}, Na^+, K^+, Mg^{2+},

Table 1 Comparisons of the responses of some HA sensors constructed based on different modified electrodes

Electrode[a]	Detection limit (μM)	Sensitivity (μA/mM)	Linear range (μM)	Reference
ARS/GCE	7.2	73.9	10–800	[33]
RuON–GCE	0.45	–	4.0–33.8	[35]
		–	33.8–78.3	
RMWCNT/GCE	1.0	28.8	1–33.8	[38]
		25	33.8–81.7	
ZnO/MWCNTs/GCE	0.12	7.5	0.4–19,000	[39]
NiCoHCF/GCE	0.23	4.94	20–200	[40]
			200–10,000	
GNPs/PPy/GCE	0.045	54.45	0.45–1,200	This work
		26.15	1,200–19,000	

[a] Alizarine red S (ARS) as a homogenous mediator, *RuON–GCE* ruthenium oxide nanoparticles glassy carbon electrode, *RMWCNT/GCE* rutin multi-wall carbon nanotubes–modified glassy carbon electrode, *ZnO/MWCNTs/GCE* ZnO nanofilms attached multi-walled carbon nanotubes–modified glassy carbon electrodes, *NiCoHCF/GCE* hybrid nickel–cobalt hexacyanoferrate film–modified glassy carbon electrode

Ca^{2+}, Ba^{2+}, Cu^{2+}, Ni^{2+}, Zn^{2+}, Fe^{3+}, Fe^{2+}, and Al^{3+}, 120-fold quantities of glucose, sucrose, fructose, oxalic acid, tartaric acid, citric acid, and malic acid, 20-fold quantities of L-tyrosine, L-arginine, and L-glutamic acid.

Sample analysis

The utilization of the proposed GNPs/PPy/GCE in a real sample was investigated by measuring HA in distilled water. The standard addition method was used for the analysis of the prepared samples. Five distilled water samples were spiked with different standard concentrations of HA. Two milliliters of this solution was placed into an electrochemical cell for analyzing HA under optimized conditions using the above technique. As shown in Table 2, the obtained results present satisfactory recovery, indicating that the proposed methods can be efficiently used for HA determination.

Reproducibility and stability

The reproducibility of the electrocatalytic effect of GNPs/PPy/GCE was tested by repetitive recording of CVs in 10 μM HA solution. It was found that the relative standard deviation (R.S.D.) of the oxidation current for 20 replicate determinations was 3.1%. Five pieces of the proposed electrode were prepared and the R.S.D. for the individual determination was 3.6%. These results indicated that the designed electrode had excellent reproducibility and anti-fouling ability.

The stability of the GNPs/PPy/GCE was studied by monitoring the remained amount of current response after successive potential cycling the modified electrode in the potential range of −0.2–0.5 V in 0.1 M PBS for 200 cycles. The peak current retained 94% of its initial value and no obvious potential shift was observed. Furthermore, the storage ability of the proposed electrode was also investigated, which stored in 0.1 M PBS (pH 7.0) at 4 °C. The current response of HA was 8% decrease of its initial value in the first 20 days and about 18% decrease after 2 months. Under the selected conditions, the method showed the GNPs/PPy/GCE had good reproducibility and stability. The high stability of the sensor can be attributed to the PPy matrix, which could increases the effective surface area of the proposed electrode and stabilize the activity of GNPs.

Conclusions

In summary, an electrochemical HA sensor was successfully fabricated by electrodeposition of GNPs with diameter of 8 nm onto pre-synthesized PPy nanoparticles matrix. The PPy nanoparticles not only help to immobilize GNPs onto the electrode surface due to the porous nanostructure and large effective surface area, but also can enhance the electron transfer rate. The GNPs/PPy/GCE exhibited excellent electrocatalytic behavior towards HA oxidation in neutral buffer solution. The positive effect can be attributed to uniform dispersion and high utilization of the metal nanoparticles on PPy supporting material. The proposed electrode showed wide linear range with two segments and low detection limit of 0.045 μM. The sensor also had a good stability, reproducibility, and anti-interference ability. The strategy of the combination of conducting PPy and GNPs presented significant advantages of synergistic effect of organic polymer and metal nanoparticles.

Table 2 Recovery of HA from distilled water samples

Sample Distilled water	HA added (μM)	HA found [a](μM)	Recovery (%)	R.S.D. (%)
1	10.0	9.7±0.5	97	3.1
2	20.0	20.2±0.4	101	2.8
3	30.0	29.7±0.5	99	3.3
4	40.0	40.7±0.3	102	3.2
5	50.0	50.4±0.4	101	2.9

[a] Average of ten determinations

Acknowledgments This work was supported by Program for New Century Excellent Talents in University (NCET-10-883), Program for Professor of Special Appointment (Eastern Scholar) at Shanghai Institutions of Higher Learning, the Specialized Research Fund for Shanghai Second Polytechnic University (XQD208014), and Excellent Young Scholars Research Fund of Shanghai (egd08014).

References

1. Zhou YG, Yang S, Qian QY, Xia XH (2009) Electrochem Commun 11:216–219
2. Tsierkezos NG, Ritter U (2010) J Solid State Electrochem 14:1101–1107
3. Hong WJ, Bai H, Xu YX, Yao ZY, Gu ZZ, Shi GQ (2010) J Phys Chem C 114:1822–1826
4. Yu JX, Rance GA, Khlobystov AN (2009) J Mater Chem 19:8928–8935
5. Kannan P, John SA (2010) Anal Chim Acta 663:158–164
6. Hosseini M, Momeni MM (2010) J Solid State Electrochem 14:1109–1115
7. Daniel MC, Astruc D (2004) Chem Rev 104:293–346
8. Liu Q, Nayfeh MH, Yau ST (2010) J Power Sources 195:3956–3959
9. Che X, Yuan R, Chai YQ, Ma LP, Li WJ, Li JJ (2009) Microchim Acta 167:159–165
10. Wei T, Luo GL, Fan ZJ, Zheng C, Yan J, Yao CZ, Li WF, Zhang C (2009) Carbon 47:2296–2299
11. Joseph S, McClure JC, Sebastian PJ, Moreira J, Valenzuela E (2008) J Power Sources 177:161–166
12. Yang XM, Li L, Yan F (2010) Sens Actuators B 145:495–500
13. Mavinakuli P, Wei SY, Wang Q, Karki AB, Dhage S, Wang Z, Young DP, Guo ZH (2010) J Phys Chem C 114:3874–3882
14. Mallouki M, Tran-Van F, Sarrazin C, Chevrot C, Fauvarque JF (2009) Electrochim Acta 54:2992–2997
15. Li M, Wei ZX, Jiang L (2008) J Mater Chem 18:2276–2280
16. Kim HS, Park DH, Lee YB, Kim DC, Kim HJ, Kim J, Joo J (2007) Synth Met 157:910–913
17. Ekanayake EMIM, Preethichandra DMG, Kaneto K (2007) Biosens Bioelectron 23:107–113
18. Li XG, Hou ZZ, Huang MR, Moloney MG (2009) J Phys Chem C 113:21586–21595
19. Park H, Kim Y, Choi YS, Hong WH, Jung D (2008) J Power Sources 178:610–619
20. Selvaraj V, Alagar M (2007) Electrochem Commun 9:1145–1153
21. Huang K, Zhang YJ, Han DX, Shen YF, Wang ZJ, Yuan JH, Zhang QX, Niu L (2006) Nanotechnology 17:283–288
22. Vasilyeva SV, Vorotyntsev MA, Bezverkhyy I, Lesniewska E, Heintz O, Chassagnon R (2008) J Phys Chem C 112:19878–19885
23. Fernando PN, Egwu IN, Hussain MS (2002) J Chromatogr A 956:261–270
24. Hofman T, Lees H (1953) Biochem J 54:579–583
25. Smith RP, Layne WR (1969) J Pharmacol Exp Ther 165:30–35
26. Kolasa T, Wardencki W (1974) Talanta 21:845–857
27. Veena K, Narayana B (2010) Oxid Commun 33:54–61
28. George M, Nagaraja KS, Balasubramanian N (2008) Chem Anal 53:315–322
29. Hu S, Zhang M, Pang DW, Cheng JK (2000) Anal Sci 16:807–810
30. Seike Y, Fukumori R, Senga Y, Oka H, Fujinaga K, Okumura M (2004) Anal Sci 20:139–142
31. Zhao C, Song JF (2001) Anal Chim Acta 434:261–267
32. Ravichandran K, Baldwin RP (1983) Anal Chem 55:1782–1786
33. Ardakani MM, Karimi MA, Mirdehghan SM, Zare MM, Mazidi R (2008) Sens Actuators B 132:52–59
34. Rosca V, Beltramo GL, Koper MTM (2004) J Phys Chem B 108:8294–8304
35. Zare HR, Hashemi SH, Benvidi A (2010) Anal Chim Acta 668:182–187
36. Shervedani RK, Bagherzadeh M (2008) Electrochim Acta 53:6293–6303
37. Bard AJ, Faulkner LR (2001) Electrochemical Methods:Fundamentals and Applications. John Wiley, New York
38. Zare HR, Sobhani Z, Mazloum-Ardakani M (2007) Sens Actuators B 126:641–647
39. Zhang CH, Wang GF, Liu M, Feng YH, Zhang ZD, Fang B (2010) Electrochim Acta 55:2835–2840
40. Shi LH, Wu T, He P, Li D, Sun CY, Li JH (2005) Electroanalysis 17:2190–2194